Original Article

Experimental application of pulsed laser-induced water jet for endoscopic submucosal dissection: Mechanical investigation and preliminary experiment in swine

Chiaki Sato,[1] Toru Nakano,[1] Atsuhiro Nakagawa,[2] Masato Yamada,[1] Hiroaki Yamamoto,[3] Takashi Kamei,[1] Go Miyata,[1] Akira Sato,[1] Fumiyoshi Fujishima,[5] Masaaki Nakai,[4] Mitsuo Niinomi,[4] Kazuyoshi Takayama,[3] Teiji Tominaga[2] and Susumu Satomi[1]

[1]*Division of Advanced Surgical Science and Technology,* [2]*Department of Neurosurgery, Tohoku University Graduate School of Medicine,* [3]*Interdisciplinary Shock Wave Application Research Division, Institute of Fluid Science,* [4]*Department of Biomaterial Science, Institute for Material Science, Tohoku University and* [5]*Department of Pathology, Tohoku University School of Medicine, Sendai, Japan*

Background and Aim: A current drawback of endoscopic submucosal dissection (ESD) for early-stage gastrointestinal tumors is the lack of instruments that can safely assist with this procedure. We have developed a pulsed jet device that can be incorporated into a gastrointestinal endoscope. Here, we investigated the mechanical profile of the pulsed jet device and demonstrated the usefulness of this instrument in esophageal ESD in swine.

Methods: The device comprises a 5-Fr catheter, a 14-mm long stainless steel tube for generating the pulsed water jet, a nozzle and an optical quartz fiber. The pulsed water jet was generated at pulse rates of 3 Hz by irradiating the physiological saline (4°C) within the stainless steel tube with an holmium-doped yttrium-aluminum-garnet (Ho:YAG) laser at 1.1 J/pulse. Mechanical characteristics were evaluated using a force meter. The device was used only for the part of submucosal dissection in the swine ESD model. Tissues removed using the pulsed jet device and a conventional electrocautery device, and the esophagus, were histologically examined to assess thermal damage.

Results: The peak impact force was observed at a stand-off distance of 40 mm (1.1 J/pulse). ESD using the pulsed jet device was successful, as the tissue specimens showed precise dissection of the submucosal layer. The extent of thermal injury was significantly lower in the dissected bed using the pulsed jet device.

Conclusion: The results showed that the present endoscopic pulsed jet system is a useful alternative for a safe ESD with minimum tissue injury.

Key words: early esophageal tumor, endoscopic submucosal dissection (ESD), holmium-YAG laser, medical engineering, minimally invasive surgery, therapeutic endoscopy

INTRODUCTION

ENDOSCOPIC SUBMUCOSAL DISSECTION (ESD)[1] is an emerging, minimally invasive therapeutic technique for en bloc resection of gastrointestinal tract lesions, including early-stage esophageal cancer. In spite of the advantages of ESD over conventional techniques, such as endoscopic mucosal resection (EMR), it requires highly advanced techniques and a learning curve exists for the performance of ESD; it has been estimated that endoscopists need to operate on 30 patients under the supervision of an expert to overcome this learning curve.[2,3] In addition, lack of instruments that can assist in this procedure without the risk of potential complications (thermal injury and vascular damage) is one of the drawbacks of the current ESD technique.[4] Therefore, new equipment that will facilitate the accomplishment of ESD without requiring special training and minimizing the risk of complications is highly desirable.

Water jet technology, based on conventional pressure-driven continuous jet[5,6] or laser/electrically induced pulsed pressure,[7–9] provides an alternative method for dissecting soft tissues without damaging small vessels or causing mechanical and thermal damage. Moreover, precise tissue dissection together with preservation of vessels and nerves can be

Corresponding: Toru Nakano, Division of Advanced Surgical Science and Technology, Tohoku University Graduate School of Medicine, 1-1, Seiryo-machi, Aoba-ku, Sendai, Miyagi 980-8574, Japan. Email: torun@med.tohoku.ac.jp
Received 30 December 2011; accepted 1 August 2012.

achieved.[10,11] Conventional pressure-driven continuous water jet technology has already been applied for endoscopic treatment.[12] However, its use was limited to transmucosal injection of water into the submucosal layer to elevate the mucosa in preparation for EMR rather than for tissue dissection,[13,14] probably due to the continuous nature of the water jet. The use of continuous water flow also carries the potential risk of obscuring the narrow endoscopic operative view.

Pulsed laser-induced water jet is a novel alternative to achieve tissue dissection with a significantly lower amount of water.[15] We have already achieved significant reduction of intraoperative blood loss and procedure time in the field of neurosurgery, despite a significant increase in the tumor removal rate.[9] The pulsed laser-induced water jet device enables tissue dissection without thermal damage while preserving small vessels.[15,16] Therefore, we have developed the endoscopic pulsed jet system for ESD. The purposes of the present study are to develop a device that can be incorporated into a gastrointestinal endoscope, to clarify the mechanical profile of the pulsed jet from this device, and to demonstrate its usefulness in ESD carried out in a swine model.

METHODS

Pulsed jet device for gastrointestinal endoscopes

FIGURE 1A IS a schematic diagram of the pulsed laser-induced jet system. Figure 1B is a photograph of the pulsed jet device and tip of the nozzle. The device consists of a 5-Fr catheter (RH-5AP4561; Terumo Corporation, Tokyo, Japan) incorporating a jet generator made of a stainless steel tube (19-G stainless steel tube, 0.9 mm internal ø, 1.26 mm external ø, length 14 mm, SUS304; Techno Science, Sendai, Japan) and an optical quartz fiber (400 μm core ø, NO.QL-400–850-5; Sparkling Photon, Tokyo, Japan), leading into a polytetrafluoroethylene (PTFE) tapered nozzle (exit 0.5 mm internal ø, inlet 1 mm internal ø). Two PTFE tubes (7–306-01 and 7–306-02; AZ One Corp., Osaka, Japan) (Fig. 1B left, bottom) were combined. This device was assembled from the distal end in the following order: the PTFE tubes, stainless steel tube, and 5-Fr catheter. The inner capillary structure was placed in the proximal end of the metal tube to prevent reverse water jet flow and thereby improve the impact force of the pulsed jet (Fig. 1A). The internal diameter of the tube was tapered from 1 mm at the entry to 0.5 mm at the exit. Because this system is intended to be incorporated into a gastrointestinal endoscope, the length of the metal tube was 14 mm to preserve the flexibility of the gastrointestinal endoscope. The proximal end of the catheter was sealed with a Y connector (AP-YC25S; Terumo Corporation) to prevent air from entering the system. Cold physiological saline (4°C) was supplied at 100 mL/h through an inner capillary by a syringe pump (TE-331S; Terumo Corporation) (Fig. 1B). Physiological saline was kept at 4°C to prevent thermal damage.[16]

The jet energy source was a pulsed holmium-doped yttrium-aluminum-garnet (Ho:YAG) laser system (model

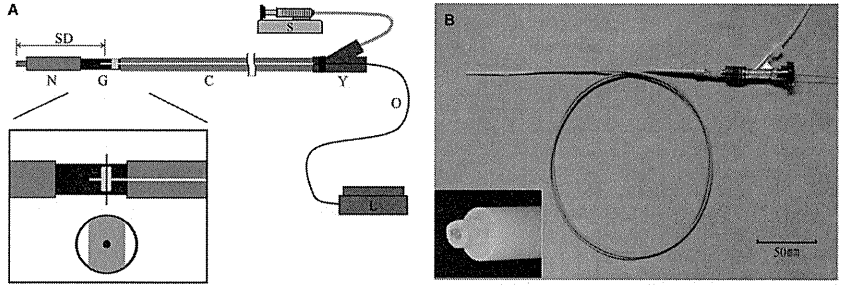

Figure 1 (A) Schematic diagram of the laser-induced pulsed jet system. N, nozzle (exit; 0.5 mm inner ø, 1.0 mm outer ø, inlet; 1.0 mm inner ø, 2.0 mm outer ø); G, pulsed jet generator made of stainless steel tube; C, Flexible catheter (0.9 mm inner ø); O, optical quartz fiber (0.4 mm core ø); Y, Y-connector; S, syringe pump; SD, stand-off distance; L, pulsed holmium-doped yttrium-aluminum-garnet (Ho:YAG) laser system. Inset: lateral sectional view (upper) and cross-sectional view (lower) of the pulsed jet generator. (B) Photograph of the laser-induced pulsed water jet device. Inset: Photograph of the nozzle. Two polytetrafluoroethylene tubes were combined. Tip of nozzle was tapered (exit: 0.5 mm inner ø, inlet: 1.0 mm outer ø).

SLS-HO; Sparkling Photon, Tokyo, Japan) with a wavelength of 2.1 μm, pulse duration of 350 μs.

Measurement of mechanical profiles

The dynamics of the jet was initially confirmed using a high-speed camera (HPV-1; Shimadzu Corporation, Kyoto, Japan). The mechanical profile of the pulsed liquid jet generated by the endoscopic pulsed jet system was evaluated using a force meter (PFDT-200GF; Sparkling Photon). The nozzle of the endoscopic pulsed jet device was placed perpendicular to the force meter using a holder and the tip of the nozzle was placed 10 mm away. The impact force of the jet was calculated with software that analyzed the time sequence observation of the impact of a single shot detected by the force meter and demonstrated on the oscilloscope (TDS3014B; Tektronix, Tokyo, Japan). The relationship between the stand-off distance (the distance between the tip of the nozzle and the optical fiber), laser energy and impact force of the liquid jet was evaluated. The stand-off distance was changed from 20 to 150 mm by 20 mm increments according to previous experiments.[8]

Esophageal ESD in swine

Three domestic pigs (*Sus scrofa domesticus* LWD, 12–14 weeks old, 30–40 kg) were used in this study. All animal procedures and protocols were approved by the institutional review board of the Center for Laboratory Animal Research of Tohoku University.

The endoscopic pulsed jet was applied at a frequency of 3 Hz and at a laser energy of 1.1 J/pulse. The stand-off distance was fixed at 100 mm. Cold physiological saline (4°C) was supplied at a rate of 100 mL/h using a syringe pump. Parameter settings were derived in preliminary experiments in which various stand-off distances and laser energy were examined at the time of dissection of resected swine esophagus (data not shown).

The pulsed jet device was incorporated into a gastrointestinal endoscope (GIF-Q260; Olympus Medical Systems, Tokyo, Japan) and esophageal ESD was carried out in healthy domestic pigs under general anesthesia with controlled ventilation. They were anesthetized with 0.04 mg/kg medetomidine chloride, 0.4 mg/kg midazolam and 0.2 mg buprenorphine hydrochloride. Isoflurane gas was used for maintenance of anesthesia during the procedure (model PH-3F; Acoma Co., Tokyo, Japan) under mechanical ventilation (ARF-900; Acoma Co.). Vital signs including blood pressure and oxygen saturation were monitored. Tissue specimens were extirpated by conventional methods [electrocautery device (KD-620LR; Olympus Medical Science Corporation, Tokyo, Japan)] (control group) and by the pulsed jet device (pulsed jet group). First, each target area (simulated lesion) was similarly marked with electrocautery in both groups. In the pulsed jet group, targets were marked at 40 cm from the dental arch, and in the control group, targets were marked at 30 cm. Then, after submucosal injection of physiological saline combined with 0.4% indigocarmine to separate the target tissue from the muscularis propria, initial cuts (so-called pre-cuts) were carried out into the submucosal layer with an electrocautery system (SurgiStat™ II; Covidien Co., Mansfield, MA, USA) in cutting mode at 100 W. In both groups, a circumferential incision into the submucosa around the lesion was made outside the initial marking using the electrocautery device in coagulation mode at 60 W. The submucosal dissection was carried out with an electrocautery device in the control group, and with the pulsed jet device in the pulsed jet group. Otherwise, procedures were all the same in both groups. In the present study, the pulsed jet device was used only for dissecting the submucosa. The operative endoscopic view of submucosal dissection with the endoscopic pulsed jet device is shown in Figure 2. The pulsed jet device has no hemostatic ability; to control bleeding, a hemostatic device (FD-410LR; Olympus Medical Science Corporation) was used in coagulation mode at 60 W in both procedures. The swine were killed after ESD by both methods; each resection bed was cut into pieces 3 mm wide and the fixed specimens were embedded in paraffin blocks, then cut parallel to the longitudinal side into sections 3 μm thick. Each section was stained with hematoxylin-eosin and elastica-Masson stain before

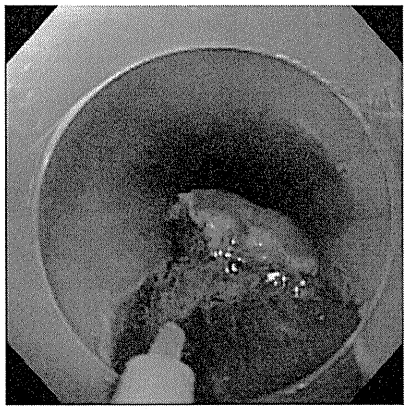

Figure 2 Operative endoscopic view of submucosal dissection with endoscopic pulsed jet device.

examination by optical microscopy to evaluate the morphological characteristics of the dissection (general dissection structure and quality of the dissection margins). Degeneration of muscle fibers (alteration of architecture, nonhomogeneous coloration, disruption of muscle fibers) indicated thermal injury.[17] The length of degeneration of muscle fibers due to thermal injury was measured in each section.

Presence of thermal damage was compared by χ^2-test. The extent of thermal damage and dissection was measured in each specimen. The extent of thermal damage in the muscular layer and the length of the dissected mucosal layer in each specimen were calculated and compared by Mann–Whitney *U*-test. The level of statistical significance was set at $P < 0.05$. All calculations were carried out using StatView J-5.0 (SAS Institute, Cary, NC, USA).

RESULTS

Measurement of mechanical profiles

FIGURE 3 SHOWS the relationship between stand-off distance and impact force of the jet at 1.1 J/pulse. In the present experiment, the peak impact force was 3.13 ± 1.22 N at the stand-off distance of 40 mm. However, an appropriate setting for dissection of swine esophagus was 1.3 ± 0.9 N at the stand-off distance of 100 mm. This setting was derived from preliminary experiments in which various stand-off distances and laser energy were examined at the

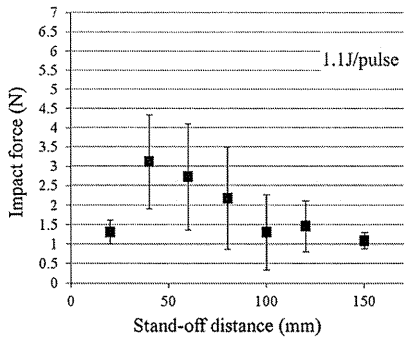

Figure 3 Relationship between stand-off distance and maximum jet impact force at a laser energy of 1.1 J/pulse. The peak of impact force at a laser energy of 1.1 J/pulse was observed at a stand-off distance of 40 mm.

time of dissection of resected swine esophagus (data not shown). The impact force of the jet increased in proportion to the increase of the laser energy (data not shown). Capillary structure increased the impact force of the jet approximately by 200% (data not shown).

Esophageal ESD in swine

Endoscopic submucosal dissection using the pulsed jet device was successful. The impact force of the pulsed jet was strong enough to dissect the submucosal layer (1.1 J/pulse and stand-off distance 100 mm, impact force 1.3 ± 0.9 N), while preserving small vessels and causing no harmful bleeding. Electrocautery device was only used to coagulate these isolated small vessels in the pulsed jet group. The endoscopic view of the surgical field was acceptable, as it was kept clean and showed that the pulsed jet device could dissect the submucosa while in contact with it or 2 to 3 mm apart from it.

A total of six ESD procedures were carried out (three by electrocautery device, three by pulsed jet device). The mean diameter of the resected mucosa did not differ significantly between the pulsed jet group and the control group (20.0 ± 8.7 mm, 21.0 ± 12.1 mm, $P = 0.9$). In both groups, specimens were dissected just on the surface of the muscle layer as shown in Figure 4. Macroscopic thermal damage in the pulsed jet group was less than that in the control group in the submucosal side of the resected specimens (Fig. 5). The en bloc resection rate was 100% in both groups. The duration of the procedure in the pulsed jet group was 50.7 ± 29.9 min, and in the control group it was 31.3 ± 16.4 min ($P = 0.38$). There was no uncontrollable bleeding or perforation in any ESD procedure. Thermal damage of the resection bed differed depending on the tissue surface (Fig. 4). Figure 4a–d shows degeneration of the inner muscularis propria (alteration of architecture of muscle fibers, nonhomogeneous coloration). ESD using the pulsed jet device resulted in almost no thermal damage to the fascia of the muscularis propria (Fig. 4e–h). Twenty-two specimens were examined in each group. The incidence of thermal damage was significantly small in 9.1% of the specimens (2/22) resected by pulsed jet compared to 59.1% (13/22) in the control group ($P = 0.004$). The extent of thermal damage of the muscle layer in relation to that of the dissected submucosal layer was significantly smaller in the pulsed jet group (1.01 ± 4.29%), compared to the control group (15.09 ± 20.60%) ($P = 0.0009$) (Fig. 6).

DISCUSSION

WE HAVE SUCCESSFULLY shown that a pulsed jet device can be incorporated into a gastrointestinal

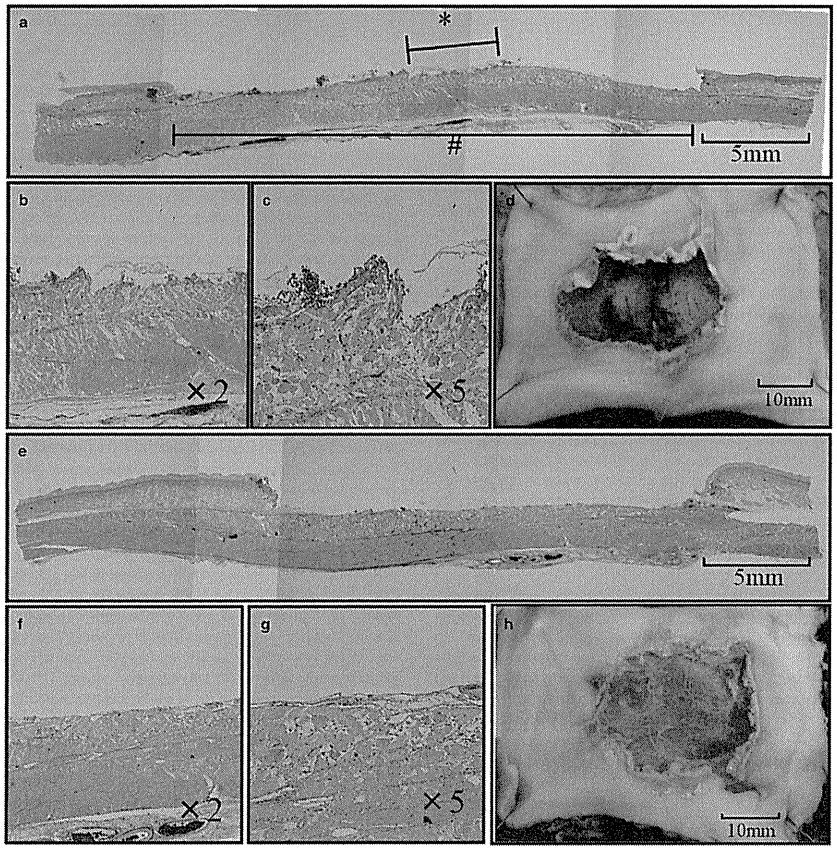

Figure 4 Microscopic (a, b, c) and macroscopic imaging (d) showing thermal damage in a specimen treated by conventional electrocautery (control group). Thermal damage was recognized at the inner circular muscle layer of the esophagus. *, Extent of thermal damage of the inner circular muscle layer. #, Extent of submucosal dissection. Elastica-Masson staining. Scale bar a: 5 mm, b: original magnification × 2, c: × 5). Microscopic (e, f, g) and macroscopic imaging (h) showing no obvious thermal damage in the specimen treated using the pulsed jet device (pulsed jet group). No obvious thermal damage was recognized in the muscle layer. Elastica-Masson staining. Scale bar e: 5 mm, f: original magnification × 2, g: × 5).

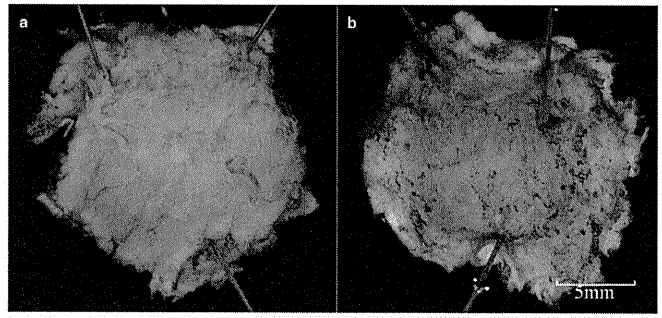

Figure 5 Photograph of resected specimens (submucosal layer side). (a) Pulsed jet group; (b) control group. Macroscopically, the submucosa of the resected specimen with the pulsed jet device has less thermal damage than that of the control group (a), whereas the submucosa of the resected specimen with the electrocautery device has thermal damage (b).

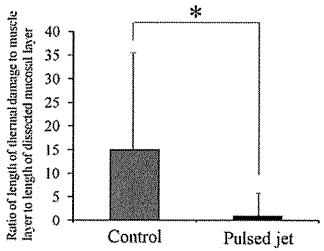

Figure 6 Extent of thermal damage of the muscle layer in relation to that of the dissected submucosal layer in both groups. The ratio of damage was 1.01% (pulsed jet group) and 15.09% (control group). *P=0.0009.

endoscope. Mechanical investigation revealed that the impact force generated by the device depended on the stand-off distance. We also showed that the pulsed jet device was safely only used for the part of submucosal dissection in the swine ESD model. There was no obvious disturbance of the surgical field by splashing, misting, or aerosol.

Water jet instrumentation, both by pressure-driven continuous jet and the present pulsed method, delivers energy as kinetic energy of the water flow, which is ejected through a small nozzle at the tip of the delivery device. The jet transmits the kinetic energy to the tissue surface and ejects particles of tissue, creating a corridor through the organ; thus, the jet can also be used for mass reduction.[5,18] The water jet instrument possesses several qualities concerning dissection that are superior to those of conventional instruments, such as selective tissue removal with vessel preservation, based on the different tensile strengths of tissues. Pressure-driven continuous water jet technology was initially used in the liver in the 1980s[5] and thereafter it has been used in neurosurgery,[19] stomach,[13] colon,[14] cardiovascular,[20] and ophthalmological[21] surgery. The use of this system in liver surgery results in reduced blood loss and less parenchymal trauma than ultrasonic aspiration or blunt dissection.[22,23] The high quality of dissections carried out with water jet and its efficacy in microsurgical procedures have been demonstrated in the field of neurosurgery.[24] Another notable advantage is the avoidance of thermal damage to the surrounding parenchyma, which is inevitable with electrocautery, electromagnetic field, ultrasonic, and laser instruments.[25,26] Despite these advantages, the size of the pressure-driven continuous water jet device and the amount of water required have prevented its incorporation into minimally invasive instruments (endoscope and catheters).

Our endoscopic pulsed jet system differs from the pressure-driven continuous water jet in its application for removal of a target lesion while preserving small vessels and using a significantly small amount of water; it allows access to deep, narrow operative fields, under either an operating microscope or a neuroendoscope.[15] The Ho:YAG laser is a solid-state laser with a mid-infrared wavelength (2.1 μm) that is close to one of the light-absorption peaks of water at 1.9 μm.[27] Therefore, the laser pulse forms a transient vapor bubble in the water flow, and the three-dimensional expansion of the confined vapor bubble is used to drive a one-dimensional liquid jet through a fine nozzle, thus generating a high-velocity pulsed jet of microliter order.[8,15] We have already reported that tissue penetration depth depends on initial velocity and pressure, which can be controlled by the laser energy, stand-off distance, and nozzle (aspect) ratio.[28,29] In the present experiment, we found that when using the

endoscopic pulsed jet device, tissue penetration also depended on those same factors, despite differences in structure.

It was reported that the performance of the pulsed jet was far superior to that of a continuous jet operating under the same parameters.[30] Seto *et al.* also reported that the degree of dissection of the pulse jet was less sensitive to exposure time, which means the pulsed jet is safe and reliable when applied for clinical treatment.[31] These findings might explain why the pulsed water jet can efficiently dissect the submucosa with less water and energy compared to the continuous water jet.

In the pulsed laser-induced water jet, the photothermal energy of the laser is transformed into kinetic energy, thus no photothermal effect occurs, and the temperature of the water jet remains below 41°C,[16] which is the reported temperature during use of the ultrasound aspirator, and is also lower than 43°C, the reported functional threshold of neuronal damage.[32] Bleeding, perforation and postoperative stricture are considered the major complications after ESD.[33] The perforation risk is even higher in the stomach,[1] esophagus[33] and colon.[34] Severe inflammation can occur after thermal damage resulting from the use of an electrocautery device. The progression of atrophy and fibrosis in the muscularis propria after inflammation could be a direct effect of damage not only of myofibers, but also of the myenteric nerve plexus.[35] The most effective and simple way to prevent perforation would be to dissect the submucosa without an electrocautery device.[36] In case of electrocoagulation hemostasis during both ESD procedures, surrounding tissues suffered not even minimal thermal damage. In previous studies, we found that a pulsed laser-induced water jet enabled the surgeon to dissect and debulk a brain tumor while preserving the small vessels down to 100 to 200 μm, which is the minimum diameter of blood vessels preserved using continuous water jet instrumentation.[15,37] Compared to conventional ESD procedures, ESD using the endoscopic pulsed jet system enables exposure of small vessels and coagulation with the electrocautery device; therefore, the number of times the electrocoagulation device is required is potentially decreased, thereby reducing thermal injury of surrounding tissues. While the pulsed jet was injected to the submucosa between 0 and 90 degrees, the muscle layer was not injured at the settings used in this study. The appropriate angle to dissect the submucosa with the pulsed jet device must be investigated in future studies. The present experiment showed that the endoscopic pulsed jet device may become an alternative to removing a target lesion, as thermal damage and the risk of perforation is significantly smaller. Consequently, the endoscopic pulsed jet system offers a new strategy for ESD.

The simplicity of the system is advantageous compared to other competing instruments. Custom-made and personal modification of the applicator with minimal costs broadens the potential future applications of this technology.[9] In the present experiments, the operative view was broader in the pulsed jet device. This was partly attributed not only to the small size of the device, but also to the use of a semi-transparent nozzle. A direct punch with the tip of the device is one of the causes of perforation. The tip of the nozzle is more flexible than the electrocautery device, reducing the risk of perforation due to direct injury.

In the present experiment, we selected the esophagus as the first organ for using the pulsed jet device, because complications of esophageal ESD could become much more serious compared to ESD of other organs in the gastrointestinal tract, such as stomach or colon. We investigated the usefulness and safety of the device in a swine esophageal ESD model. Pulsed jet device can be used in other organs (kidney, liver, stomach and colon), provided the appropriate settings for other organs are clarified in future studies.

Lack of examination of the pathological tissues (i.e. malignancy and fibrosis) and lack of long-term evaluation as well as the small number of animals used are limitations of the present study. Before this device is used in humans, additional short- and long-term animal experiments, including pathological examination, should be carried out.

ACKNOWLEDGMENTS

THIS WORK WAS supported in part by Grants-in-Aid for Scientific Research (B) (No. 18390388) and (No. 19390372), a Grant-in-Aid for Young Scientists (A) (No. 19689028), (22689039), and Challenging Exploratory Research (No. 21659313), (21659334) from the Japanese Ministry of Health, Labour and Welfare, the Japanese Foundation for Research and Promotion of Endoscopy Grant (A), the Tohoku University Exploratory Research Program for Young Scientists (ERYs), the Collaborative Research Project of the Institute of Fluid Science, Tohoku University, Ogino Award of Research Facilitating from Japanese Society of Biomedical Engineering, and SEI Group CSR Foundation.

The authors would like to thank Dr Daisuke Kudo and Kiyonobu Ohtani for valuable comments, and Teruko Sueta, Nobuko Hashimoto, and Yayoi Okano for conducting the experiments.

CONFLICT OF INTERESTS

AUTHORS DECLARE NO conflict of interests for this article.

REFERENCES

1 Gotoda T. A large endoscopic resection by endoscopic submucosal dissection procedure for early gastric cancer. *Clin. Gastroenterol. Hepatol.* 2005; **3**: S71–3.
2 Gotoda T, Friedland S, Hamanaka H, Soetikno R. A learning curve for advanced endoscopic resection. *Gastrointest. Endosc.* 2005; **62**: 866–7.
3 Choi IJ, Kim CG, Chang HJ, Kim SG, Kook MC, Bae JM. The learning curve for EMR with circumferential mucosal incision in treating intramucosal gastric neoplasm. *Gastrointest. Endosc.* 2005; **62**: 860–5.
4 Oda I, Gotoda T, Hamanaka H *et al.* Endoscopic submucosal dissection for early gastric cancer: Technical feasibility, operation time and complication from a large consecutive series. *Dig. Endosc.* 2005; **17**: 54–8.
5 Papachristou DN, Barters R. Resection of the liver with a water jet. *Br. J. Surg.* 1982; **69**: 93–4.
6 Oertel J, Gaab MR, Warzok R, Piek J. Waterjet dissection in the brain: Review of the experimental and clinical data with special reference to meningioma surgery. *Neurosurg. Rev.* 2003; **26**: 168–74.
7 Miller JM, Palanker DV, Vankov A, Marmor MF, Blumenkranz MS. Precision and safety of the pulsed electron avalanche knife in vitreoretinal surgery. *Arch. Ophthalmol.* 2003; **121**: 871–7.
8 Hirano T, Komatsu M, Saeki T *et al.* Enhancement of fibrinolytics with a laser-induced liquid jet. *Lasers Surg. Med.* 2001; **29**: 360–8.
9 Ogawa Y, Nakagawa A, Takayama K, Tominaga T. Pulsed laser-induced liquid jet for skull base tumor removal with vascular preservation through the transsphenoidal approach: A clinical investigation. *Acta Neurochir. (Wien)* 2011; **153**: 823–30.
10 Piek J, Oertel J, Gaab MR. Waterjet dissection in neurosurgical procedures: Clinical results in 35 patients. *J. Neurosurg.* 2002; **96**: 690–6.
11 Tschan C, Gaab MR, Krauss JK, Oertel J. Waterjet dissection of the vestibulocochlear nerve: An experimental study. *J. Neurosurg.* 2009; **110**: 656–61.
12 Neuhaus H, Wirths K, Schenk M, Enderle MD, Schumacher B. Randomized controlled study of EMR versus endoscopic submucosal dissection with a water-jet hybrid-knife of esophageal lesions in a porcine model. *Gastrointest. Endosc.* 2009; **70**: 112–20.
13 Kaehler GF, Sold MG, Fischer K, Post S, Enderle M. Selective fluid cushion in the submucosal layer by water jet: Advantage for endoscopic mucosal resection. *Eur. Surg. Res.* 2007; **39**: 93–7.
14 Yahagi N, Neuhaus H, Schumacher B *et al.* Comparison of standard endoscopic submucosal dissection (ESD) versus an optimized ESD technique for the colon: An animal study. *Endoscopy* 2009; **41**: 340–5.
15 Ohki T, Nakagawa A, Hirano T *et al.* Experimental application of pulsed Ho : YAG laser-induced liquid jet as a novel rigid neuroendoscopic dissection device. *Lasers Surg. Med.* 2004; **34**: 227–34.
16 Hirano T, Nakagawa A, Uenohara H *et al.* Pulsed liquid jet dissector using holmium:YAG laser–a novel neurosurgical device for brain incision without impairing vessels. *Acta Neurochir. (Wien)* 2003; **145**: 401–6. discussion 406.
17 Lequerica JL, Sanz E, Hornero F *et al.* Esophagus histological analysis after hyperthermia-induced injury: Implications for cardiac ablation. *Int. J. Hyperthermia* 2009; **25**: 150–9.
18 Oertel J, Gaab MR, Knapp A, Essig H, Warzok R, Piek J. Water jet dissection in neurosurgery: Experimental results in the porcine cadaveric brain. *Neurosurgery* 2003; **52**: 153–9. discussion 159.
19 Terzis AJ, Nowak G, Rentzsch O, Arnold H, Diebold J, Baretton G. A new system for cutting brain tissue preserving vessels: Water jet cutting. *Br. J. Neurosurg.* 1989; **3**: 361–6.
20 Aroussi AA, Sami IM, Leguerrier A, Verhoye JP. The blower: A useful tool to complete thrombectomy of the mechanical prosthetic valve. *Ann. Thorac. Surg.* 2006; **81**: 1911–2.
21 Lipshitz I, Bass R, Loewenstein A. Cutting the cornea with a waterjet keratome. *J. Refract. Surg.* 1996; **12**: 184–6.
22 Izumi R, Yabushita K, Shimizu K *et al.* Hepatic resection using a water jet dissector. *Surg. Today* 1993; **23**: 31–5.
23 Rau HG, Duessel AP, Wurzbacher S. The use of water-jet dissection in open and laparoscopic liver resection. *HPB (Oxford)* 2008; **10**: 275–80.
24 Oertel J, Gen M, Krauss JK, Zumkeller M, Gaab MR. The use of waterjet dissection in endoscopic neurosurgery. Technical note. *J. Neurosurg.* 2006; **105**: 928–31.
25 Oertel J, Gaab MR, Pillich DT, Schroeder HW, Warzok R, Piek J. Comparison of waterjet dissection and ultrasonic aspiration: An in vivo study in the rabbit brain. *J. Neurosurg.* 2004; **100**: 498–504.
26 Schurr MO, Wehrmann M, Kunert W *et al.* Histologic effects of different technologies for dissection in endoscopic surgery: Nd:YAG laser, high frequency and water-jet. *Endosc. Surg. Allied Technol.* 1994; **2**: 195–201.
27 Jansen ED, van Leeuwen TG, Motamedi M, Borst C, Welch AJ. Temperature dependence of the absorption coefficient of water for midinfrared laser radiation. *Lasers Surg. Med.* 1994; **14**: 258–68.
28 Nakagawa A, Hirano T, Komatsu M *et al.* Holmium: YAG laser-induced liquid jet knife: Possible novel method for dissection. *Lasers Surg. Med.* 2002; **31**: 129–35.
29 Nakagawa A, Kumabe T, Kanamori M *et al.* Clinical application of pulsed laser-induced liquid jet: Preliminary report in glioma surgery. *Neurol. Surg.* 2008; **36**: 1005–10. [Article in Japanese].
30 Foldyna J, Sitek L, Svehla B, Svehla S. Utilization of ultrasound to enhance high-speed water jet effects. *Ultrason. Sonochem.* 2004; **11**: 131–7.
31 Seto T, Yamamoto H, Takayama K, Nakagawa A, Tominaga T. Characteristics of an actuator-driven pulsed water jet generator to dissecting soft tissue. *Rev. Sci. Instrum.* 2011; **82**: 055105.

32 Matsumi N, Matsumoto K, Mishima N *et al.* Thermal damage threshold of brain tissue–histological study of heated normal monkey brains. *Neurol. Med. Chir. (Tokyo)* 1994; **34**: 209–15.
33 Fujishiro M, Yahagi N, Kakushima N *et al.* Endoscopic submucosal dissection of esophageal squamous cell neoplasms. *Clin. Gastroenterol. Hepatol.* 2006; 4: 688–94.
34 Taku K, Sano Y, Fu KI *et al.* Iatrogenic perforation associated with therapeutic colonoscopy: A multicenter study in Japan. *J. Gastroenterol. Hepatol.* 2007; **22**: 1409–14.
35 Honda M, Nakamura T, Hori Y *et al.* Process of healing of mucosal defects in the esophagus after endoscopic mucosal resection: Histological evaluation in a dog model. *Endoscopy* 2010; **42**: 1092–5.
36 Yamasaki M, Kume K, Yoshikawa I, Otsuki M. A novel method of endoscopic submucosal dissection with blunt abrasion by submucosal injection of sodium carboxymethylcellulose: An animal preliminary study. *Gastrointest. Endosc.* 2006; **64**: 958–65.
37 Nakagawa A, Hirano T, Jokura H *et al.* Pulsed holmium:yttrium-aluminum-garnet laser-induced liquid jet as a novel dissection device in neuroendoscopic surgery. *J. Neurosurg.* 2004; **101**: 145–50.

Hepatology Research

Hepatology Research 2014; 44: 238–245 doi: 10.1111/hepr.12102

Short Communication

Eradication of hepatitis C virus could improve immunological status and pyoderma gangrenosum-like lesions

Yasuteru Kondo,[1] Tomoaki Iwata,[1] Takahiro Haga,[2] Osamu Kimura,[1] Masashi Ninomiya,[1] Eiji Kakazu,[1] Takayuki Kogure,[1] Tatsuki Morosawa,[1] Setsuya Aiba[2] and Tooru Shimosegawa[1]

Divisions of [1]Gastroenterology and [2]Dermatology, Tohoku University Hospital, Sendai, Japan

Hepatitis C virus (HCV) can affect immune cells and induce various kinds of immune-related diseases including pyoderma gangrenosum. We experienced a difficult-to-treat case of pyoderma gangrenosum-like lesions in a patient with HCV infection. The patient was treated with pegylated interferon (PEG IFN)-α-2b and ribavirin (RBV) therapy and achieved a sustained virological response. Before the eradication of HCV, the frequency of T-helper 17 cells was remarkably high in comparison to chronic hepatitis C patients without extrahepatic immune-related diseases. Moreover, we could detect negative and positive strand-specific HCV RNA in the CD19$^+$ B lymphocytes and CD4$^+$ T lymphocytes. However, after the eradication of HCV, the immunological status became normal and the pyoderma gangrenosum-like lesions became stable without immunosuppressive therapy. Here, we report a sequential immunological analysis during PEG IFN/RBV therapy and the beneficial effect of HCV eradication in difficult-to-treat pyoderma gangrenosum-like lesions.

Key words: CD19, CD4, extrahepatic diseases, hepatitis C virus, T-helper 17

INTRODUCTION

HEPATITIS C VIRUS (HCV) is non-cytopathic virus that causes chronic hepatitis C (CHC), and hepatocellular carcinoma (HCC), a lymphoproliferative disease. Approximately 70% of those acutely infected will develop CHC.[1] Various kinds of immune cells, including CD4$^+$ T-helper (Th) cells, CD8$^+$ cytotoxic T lymphocytes (CTL), B cells, regulatory T cells (Treg) and monocytes, may be affected by persistent infection of HCV.[2–5] HCV can cause not only immunosuppression, which contributes to persistent infection, but also unfavorable immune activation, which can induce various kinds of extrahepatic manifestations, including immune-related diseases.[3,4,6,7]

The extrahepatic manifestations of CHC include mixed cryoglobulinemia that represents a prototype of HCV-associated disorders.[8–10] Mixed cryoglobulinemia is caused by various kinds of stimulation. It was reported that chronic antigenic stimulation may induce specific B-cell clones that could produce cryoglobulins. Moreover, B-cell activation and/or dysregulation could originate as a result of HCV binding to CD81 tetraspanin molecules or as a consequence of its ability to replicate in B lymphocytes.[10] A variety of skin disorders are associated with an increased level of monoclonal immunoglobulin proteins. These kinds of disorders include pyoderma gangrenosum, leukocytoclastic vasculitis pemphigus, bullous pemphigoid, epidermolysis bullosa aquisita, Sézary syndrome, lymphomatoid papulosis, urticaria pigmentosa and acquired ichthyosis.[11] We experienced a CHC patient with severe pyoderma gangrenosum-like lesions treated with immunosuppressive therapy. However, the activity of the pyoderma gangrenosum-like lesions was not improved during immunosuppressive therapy. Then, we tried eradication of HCV by using pegylated interferon (PEG IFN) and ribavirin (RBV) therapy because a relationship between CHC and pyoderma gangrenosum-like lesions was suspected.[12]

In this study, we analyzed sequentially various kinds of immune cells including activated CD3$^+$ T cells, CD4$^+$ T cells, CD8$^+$ T cells, CD19$^+$ B cells, activated B cells, Th1 cells, Th2 cells, Th17 cells and CD4$^+$ CD25$^+$ interleukin (IL)-7R$^-$ Treg. Moreover, the detection of strand-specific HCV RNA was carried out because we previously reported that lymphotropic HCV could affect T-cell commitment and immunoglobulin hypermutation.[3,4,6,7,13,14]

Correspondence: Dr Yasuteru Kondo, Division of Gastroenterology, Tohoku University Hospital, 1-1 Seiryo-machi, Aoba-ku, Sendai City, Miyagi 980-8574, Japan. Email: yasuteru@ebony.plala.or.jp
Conflict of interest: The authors declare that they have no conflict of interest.
Received 15 January 2013; revision 12 February 2013; accepted 21 February 2013.

METHODS

Patient

A CHC PATIENT with severe pyoderma gangrenosum-like lesions was enrolled in this study. The pyoderma gangrenosum-like lesions were diagnosed by the clinical phenotype and non-specific inflammation of skin lesions in the Division of Dermatology, Tohoku University Hospital. Although this patient was treated with steroid and skin transplantation, the skin condition was not improved. Therefore, we concluded that this patient needed antiviral treatment to remove the effects of HCV. Permission for the study was obtained from the Ethics Committee at Tohoku University Graduate School of Medicine (permission no. 2006-194). Written informed consent was obtained from this patient. The patient was monitored for 3 years, and peripheral blood samples were obtained and assessed during PEG IFN/RBV treatment. At each assessment, the patient was evaluated for the serum levels of HCV RNA, blood chemistry and hematology. The liver histology was analyzed by the METAVIR score at the start of PEG IFN/RBV therapy.

Detection of IL-28B polymorphism

Genomic DNA was isolated from peripheral blood mononuclear cells (PBMC) using an automated DNA isolation kit. Then, the polymorphism of IL-28B (rs8099917) was analyzed using real-time polymerase chain reaction (PCR; TaqMan SNP Genotyping Assay, Applied Biosystems, NY, USA). The detection of IL-28B polymorphism was approved by the Ethics Committee at Tohoku University Graduate School of Medicine (permission no. 2010-323)

Isolation of PBMC, CD4$^+$ T cells and CD19$^+$ B cells, and flow cytometry analysis

Peripheral blood mononuclear cells were isolated from fresh heparinized blood by means of Ficoll-Hypaque density gradient centrifugation. PBMC were stained with CD3, CD4, CD8, CD19, CD25, CD40, CD86, IL-7R and HLA-DR antibodies (BD Pharmingen, San Jose, CA, USA) for 15 min on ice to analyze the CD3$^+$ HLA-DR$^+$ cells, CD3$^+$ CD4$^+$ HLA-DR$^+$ cells, CD3$^-$ CD8$^+$ HLA-DR$^+$ cells, CD19$^+$ CD40$^+$ cells, CD19$^+$ CD86$^+$ cells and CD3$^+$ CD4$^+$ CD25$^+$ IL-7R$^-$ Treg. Isotype-matched control antibodies were used for adjustment of the fluorescence intensity. The frequencies of the immune subsets were analyzed using FACS Canto-II (BD Biosciences, San Jose, CA, USA).

IFN-γ, IL-10 and IL-17A cytokine secretion assay

Peripheral blood mononuclear cells were stimulated with CD3- and CD28-coated beads (Miltenyi Biotec, Gladbach, Germany) for 12 h. Cells were washed by adding 2 mL of cold phosphate-buffered saline and resuspended in 90 μL of cold RPMI-1640 medium. After the addition of 10 μL of IL-10, IFN-γ or IL-17A Catch Reagent (Miltenyi Biotec), cells were incubated for 5 min on ice. Thereafter, the cells were diluted with 1 mL of warm medium (37°C) and further incubated in a closed tube for 45 min at 37°C under slow, continuous rotation. The cells were washed and IL-10- or IFN-γ-secreting cells were stained by adding 10 μL of IL-10, IFN-γ or IL-17A Detection Antibody (PE conjugated or APC conjugated; Miltenyi Biotec) together with anti-CD4-PerCP.

Quantification of IL-17A, IL-21 and IL-23

The amounts of IL-17A, IL-21 and IL-23 were quantified using enzyme-linked immunosorbent assay (ELISA) kits (eBioscience, San Diego, CA, USA). The serum samples were collected at sampling points and stored at −20°C. The ELISA procedure was performed according to the manufacturer's protocol. The IL-17A, IL-21 and IL-23 sample concentrations were calculated using a standard curve.

Strand-specific intracellular HCV RNA detection

Strand-specific intracellular HCV RNA was detected using a recently established procedure that combines methods published elsewhere, with minor modification. Positive strand-specific and negative strand-specific HCV RNA were detected using a nested PCR method. Reactions were performed with 2 μL of 10 × reverse transcriptase (RT) buffer, 2 μL of 10 mmol/L magnesium chloride, 200 μmol/L each of deoxyadenosine triphosphate, deoxycytidine triphosphate, deoxygua-

nosine triphosphate, 100 μmol/L of thymidine triphosphate (dTTP), 0.2 U of uracil-N glycosylase (UNG; Perkin Elmer [Fremont, CA, USA]/Applied Biosystems, Foster City, CA, USA), 5 U of rTth DNA polymerase; and 50 pmol of strand-specific HCV primers (position according to the 5′ untranslated region), nt −285 to −256 (ACTGTCTTCACGCAGAAAGCGTCTAGCCAT) and −43 to −14 (CGAGACCTCCCGGGGCACTCG CAAGCACCC), and template RNA. The RT mixture was incubated for 10 min at room temperature and then at 70°C for an additional 15 min. The cDNA product was subjected to the first PCR with 80 μL of PCR reaction buffer containing 50 pmol of HCV downstream strand-specific primer. The PCR amplification consisted of 5 min of 95°C, followed by 35 cycles and then 7-min extension at 72°C. For the second nested PCR, an aliquot (1/10) of the first PCR reaction mixture was re-amplified using 50 pmol of each of two primers, nt −276 to −247 (ACGCAGAAAGCGTCTAGCCATGGCGT TAGT) and nt −21 to −50 (TCCCGGGGCACTCGCAAG CACCCTATCAGG), which span the 255-base pair region nt −276 to −21 of HCV RNA, and Taq polymerase (Applied Biosystems). The reaction was run for 35 cycles. Semiquantification was achieved by serial four-fold dilution. The relative titer was expressed as the highest dilution giving a visible band of the appropriate internal control; semiquantification of β-actin mRNA was performed using the same RNA extracts.

Table 1 Biochemical, hematological, virological laboratory test

Laboratory test before the immunosuppressive therapy for pyoderma gangrenosum					
WBC	7600 uL	T-Bil	0.4 mg/dL	IgG	954 mg/dL
RBC	396 10^4/ul	D-Bil	0.1 mg/dL	IgA	259 mg/dL
Hb	12.4 g/dL	ALP	294 IU/L	IgM	439 mg/dL
HCT	37.2%	γ-GTP	52 IU/L		
MCV	94 fl	AST	36 IU/L	RF	746.2 U/L
MCH	31.4 pg	ALT	39 IU/L		
MCHC	33.4%	LDH	162 IU/L	C3	81 mg/dL
PLT	297 × 10^3/uL	ChE	304 IU/L	C4	4.3 mg/dL
				CH50	27.7/mL
PT-INR	0.97	TP	6.8 g/dL		
		ALB	3.8 g/dL	Cryo	+
Na	144 mEq/L				
K	4 mEq/L	HCV RNA	6.2 log copies/mL	ANA	<79
Cl	111 mEq/L	HCV Genotype	1b	M2	5(−)
Liver histology	METAVIR A2/F2				
IL-28B SNP (rs8099917)	T/T				

Sampling points	1	2	3	4
T-Bil (mg/dL)	0.4	0.5	0.4	0.5
D-Bil (mg/dL)	0.1	0.1	0.1	0.1
ALP (IU/L)	294	419	320	322
γ-GTP (IU/L)	52	45	28	18
AST (IU/L)	36	49	24	15
ALT (IU/L)	39	40	16	11
RF (U/L)	746.2	671.5	648.5	648.5
C3 (mg/dL)	81	88	82	95
C4 (mg/dL)	4.3	6.5	7.2	9.4
CH50 (/mL)	27.7	41.2	39.8	48.2

1. Before the immunosuppressive therapy for pyoderma gangrenosum.
2. Before the PEG IFN/RBV therapy for HCV eradication.
3. Just after the PEG IFN/RBV therapy for HCV eradication.
4. Six months after the PEG IFN/RBV therapy for HCV eradication (SVR).

ALT, alanine aminotransferase; Hb, hemoglobin; PLT, platelet; RBC, red blood cell; WBC, white blood cell.

RESULTS

Clinical course of a CHC patient with pyoderma gangrenosum-like lesions

REPRESENTATIVE BIOCHEMICAL AND hematological analyses at several time points are shown (Table 1). The polymorphism of IL-28B (rs8099917) is of T/T major type. The patient (patient A) had genotype 1b and high HCV RNA titers (6.1 log copies/mL) before the immunosuppressive therapy for pyoderma gangrenosum-like lesions. Cryoglobulin could be detected at several time points. The rheumatoid factor was 746.2. The activity of the pyoderma gangrenosum-like lesions was high at this time point (Fig. 1a). Therefore, immunosuppressive therapy (cyclosporin) was started. During the immunosuppressive therapy, the activity of the pyoderma gangrenosum-like lesions did not improve. Then, we started the PEG IFN/RBV therapy to eradicate the HCV because the relevance of HCV to the pyoderma gangrenosum-like lesions was suspected. The titers of HCV RNA rapidly declined after the start of PEG IFN/RBV therapy. The patient achieved a sustained virological response (SVR) after the 48 weeks of treatment with PEG IFN/RBV. After the achievement of SVR, the pyoderma gangrenosum-like lesions rapidly improved without immunosuppressive therapy (Fig. 1a).

Strand-specific HCV RNA detection in lymphoid cells

Then, we carried out strand-specific nested PCR to detect the HCV RNA using a method previously published by

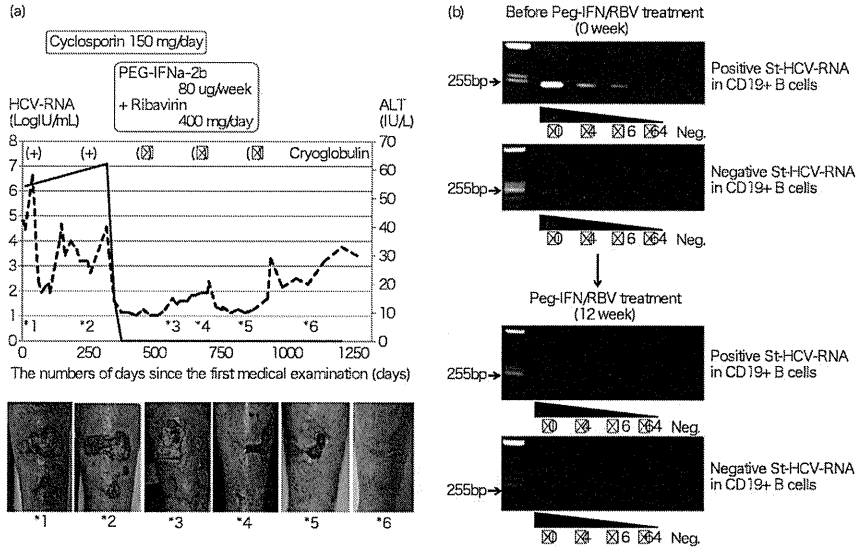

Figure 1 Clinical data and condition of the pyoderma gangrenosum-like lesions during the cyclosporin and/or pegylated interferon (PEG IFN)-α-2b/ribavirin (RBV) treatment. (a) Titers of hepatitis C virus (HCV) RNA and the level of alanine aminotransferase (ALT) are shown in the upper graph. This graph includes the positivity of cryoglobulin in the serum. Pictures of the same site of the pyoderma gangrenosum-like lesions are shown in the lower part of the figure. The numbers located at the lower part of the pictures and in the graph indicate the time points during treatment and follow up. (b) Representative polymerase chain reaction (PCR) bands that show the semiquantification of strand-specific HCV RNA detection in $CD19^+$ B cells are shown. The size of target PCR bands is 255 base pairs. For negative control, extracted HCV RNA was run in every reverse transcription PCR test without an upstream HCV primer. ——, HCV RNA; – – –, ALT.

Table 2 Detection of strand-specific HCV RNA in the $CD4^+$ T cells and $CD19^+$ B cells

	Time point	4 weeks before treatment	0 weeks	12 weeks	48 weeks
$CD4^+$ T cells	Positive St-HCV RNA	4	4	1	0
	Negative St-HCV RNA	1	1	0	0
$CD19^+$ B cells	Positive St-HCV RNA	16	16	1	0
	Negative St-HCV RNA	1	1	0	0

The titers of HCV RNA were expressed as the highest dilution giving a visible band of the correct size. The data of two independent studies had same results.
HCV, hepatitis C virus; St, strand.

our group. The detection of negative-strand HCV RNA indicates the existence of HCV RNA replication in the cells. The positive rate of negative strand lymphotropic HCV RNA among general CHC patients was approximately 10% (unpubl. data, Kondo *et al.*). We could detect positive and negative strand-specific HCV RNA in lymphoid cells ($CD4^+$ T cells and $CD19^+$ B cells) at two points before the PEG IFN/RBV treatment (Table 2) (Fig. 1b). After the eradication of HCV, we could not detect positive and negative strand-specific HCV RNA in the lymphoid cells or serum.

Sequential immunological analysis during PEG IFN/RBV treatment

We analyzed various kinds of lymphoid cells, because we previously reported that lymphotropic HCV could affect the Th commitment and proliferation.

The frequencies of activated T cells ($HLA\text{-}DR^+$ $CD3^+$, $CD4^+$ or $CD8^+$ T cells), Th1 cells (IFN-γ-secreting $CD4^+$ T cells), Th2 cells (IL-10-secreting $CD4^+$ cells), Treg ($CD4^+$ $CD25^{high}$ $IL\text{-}7R^-$ cells) and $CD19^+$ $CD40^+$ B cells were not remarkably changed during the PEG IFN/RBV treatment (Fig. 2a,b). On the other hand, the frequency of Th17 cells (IL-17A-secreting $CD4^+$ T cells) was remarkably decreased after the PEG IFN/RBV treatment (Fig. 2b). The frequency of $CD19^+$ $CD86^+$ activated B cells was slightly decreased after the PEG IFN/RBV treatment. The frequency of Th17 cells in patient A was remarkably high in comparison to those in CHC patients ($n = 5$) without extrahepatic immune-related diseases (Fig. 2c). The time point of PBMC sampling was before the PEG IFN/RBV treatment (Fig. 2c). All five CHC patients included in this study had high viral loads (>5 log copies/mL), IL-28B T/T, genotype 1b HCV RNA. All CHC patients were male. Moreover, we analyzed the amounts of Th17-related cytokines (IL-17A, IL-21 and IL-23) using ELISA. Patient A had remarkably higher amounts of these cytokines (IL-17A, IL-21 and IL-23) in comparison to the control CHC patients (Fig. 2d). Some of the control patients had lower than measurable amounts of these cytokines (Fig. 2d). Therefore, we used reference amounts of cytokines calculated using a standard curve.

DISCUSSION

IT HAS BEEN reported that various kinds of extrahepatic disease could be induced by persistent infection of HCV.[15,16] Among the extrahepatic diseases, cryoglobulin and autoimmune-related diseases including pyoderma gangrenosum were most frequently detected in CHC patients.[12,17,18] The relationship between cryoglobulin and Th17 cells has been studied in our group (unpubl. data, Kondo *et al.*).[19] It has been reported that

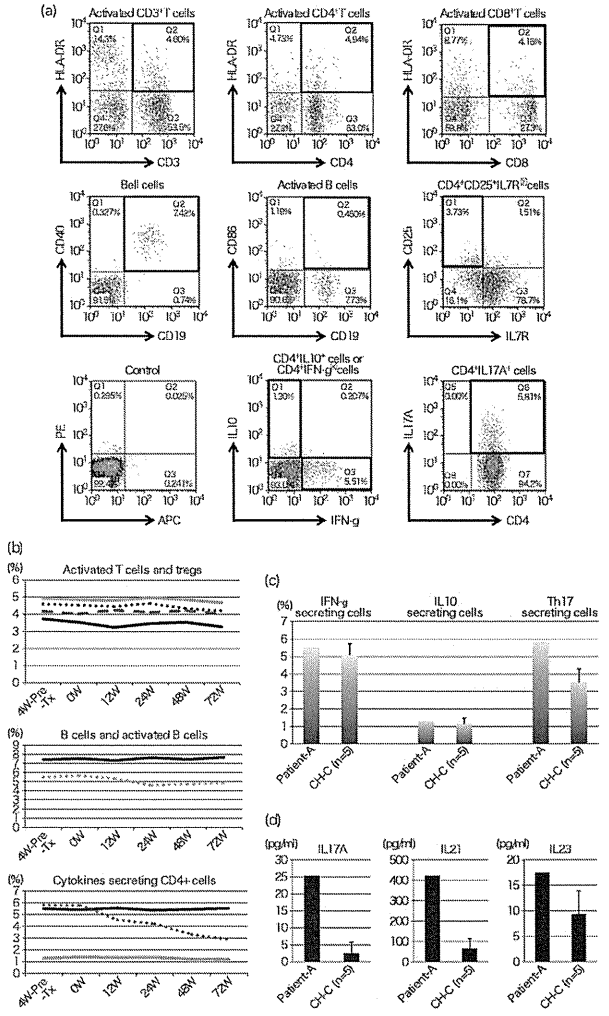

Figure 2 Immunological analysis during pegylated interferon (PEG IFN)-α-2b/ribavirin (RBV) treatment in patient A. (a) Representative dot plots indicating various kinds of immune cell subsets and cytokine-secreting cells are shown. Bold boxes indicate the target subsets in the quadrant of dot plots. (b) Sequential immunological data are shown. The frequencies of various kinds of immune cell subsets are shown. (c) The frequencies of cytokine-secreting cells were compared between patient A and chronic hepatitis C (CHC) without extrahepatic diseases ($n = 5$). (d) Amounts of interleukin (IL)-17A, IL-21 and IL-23 are shown in the bar graph. Some of the control patients had lower than measurable amounts of these cytokines. Therefore, we used reference amounts of cytokines calculated using a standard curve. Error bars indicate standard deviation. • • • •, $CD3^+$ $HLA\text{-}DR^+/CD3^+ \times 100$; ▭▭▭, $CD4^+$ $HLA\text{-}DR^+/CD4^+ \times 100$; ▭ ▭, $CD8^+$ $HLA\text{-}DR^+/CD8^+ \times 100$; ▬▬, $CD4^+$ $CD25^{high}$ $IL\text{-}7R^-/CD4^+ \times 100$; ▬▬, $CD19^+$ $CD40^+$ B cells/lymphocytes ×100; * * * *, $CD19^+$ $CD86^+$ B cells/$CD19^+ \times 100$; ▬▬, $CD4^+$ IFN-γ^+ cells/$CD4^+ \times 100$; ▭▭▭, $CD4^+$ $IL\text{-}10^+$ cells/$CD4^- \times 100$; • • • •, $CD4^+$ $IL\text{-}17A^+$ cells/$CD4^- \times 100$.

Th17 cells were associated with the immunopathogenesis of autoimmune diseases.[20–22] Previously, we reported that lymphotropic HCV could affect the commitment of helper T cells, T-cell proliferation, and immunoglobulin-hypermutation that may affect the dysregulation of the immune system.[3,4,6,13,19] The biological significance of lymphotropic HCV could be its contribution to not only the mechanism of HCV-persistent infection but also the induction of extrahepatic diseases including pyoderma gangrenosum, because cryoglobulin and the dysregulation of T cells may be involved in the pathogenesis of pyoderma gangrenosum. In patient A, the frequency of Th17 cells was remarkably decreased after the eradication of HCV. During the immunosuppressive therapy, the titers of HCV RNA slightly increased. Therefore, the modulation of the immune system directly induced by HCV had an important role in the induction of pyoderma gangrenosum-like lesions. After the eradication of HCV, the pyoderma gangrenosum-like lesions completely recovered without immunosuppressive therapy. These observations suggest that the eradication of HCV is a significant treatment option for extrahepatic diseases with dysregulation of the immune system in CHC patients. However, we could not analyze the basal level of the immune response without immunosuppressive therapy due to the lack of PBMC samples. We could not exclude the contribution of other immune cells in addition to Th17 cells to the induction of pyoderma gangrenosum-like lesions, because the administration of cyclosporin could suppress the T-cell response. The frequencies of IFN-γ- and IL-10-secreting cells in patient A were comparable to those of the CHC patients without immunosuppressive therapy. Therefore, the immune response in patient A might have been strongly activated in comparison to the CHC patients without autoimmune-related diseases.

In conclusion, we sequentially examined the existence of lymphotropic HCV and the immune response during PEG IFN/RBV treatment for difficult-to-treat pyoderma gangrenosum-like lesions. The results suggest the relevance of the frequency of Th17 cells to the activity of pyoderma gangrenosum-like lesions in CHC patients. Moreover, the existence of lymphotropic HCV may be involved in this phenomenon.

ACKNOWLEDGMENT

THIS WORK WAS supported in part by a Grant-in-Aid from the Ministry of Education, Culture, Sport, Science, and Technology of Japan (Y. K., no. 23790861).

REFERENCES

1 Alter MJ, Kruszon-Moran D, Nainan OV *et al.* The prevalence of hepatitis C virus infection in the United States, 1988 through 1994. *N Engl J Med* 1999; 341: 556–62.
2 Kondo Y, Kobayashi K, Kobayashi T *et al.* Distribution of the HLA class I allele in chronic hepatitis C and its association with serum ALT level in chronic hepatitis C. *Tohoku J Exp Med* 2003; 201: 109–17.
3 Machida K, Kondo Y, Huang JY *et al.* Hepatitis C virus (HCV)-induced immunoglobulin hypermutation reduces the affinity and neutralizing activities of antibodies against HCV envelope protein. *J Virol* 2008; 82: 6711–20.
4 Kondo Y, Machida K, Liu HM *et al.* Hepatitis C virus infection of T cells inhibits proliferation and enhances fas-mediated apoptosis by down-regulating the expression of CD44 splicing variant 6. *J Infect Dis* 2009; 199: 726–36.
5 Kondo Y, Ueno Y, Shimosegawa T. Dysfunction of immune systems and host genetic factors in hepatitis C virus infection with persistent normal ALT. *Hepat Res Treat* 2011; 2011: 713216.
6 Kondo Y, Ueno Y, Kakazu E *et al.* Lymphotropic HCV strain can infect human primary naive CD4+ cells and affect their proliferation and IFN-gamma secretion activity. *J Gastroenterol* 2011; 46: 232–41.
7 Kondo Y, Ueno Y, Shimosegawa T. Biological significance of HCV in various kinds of lymphoid cells. *Int J Microbiol* 2012; 2012: 647581.
8 Saadoun D, Landau DA, Calabrese LH, Cacoub PP. Hepatitis C-associated mixed cryoglobulinaemia: a crossroad between autoimmunity and lymphoproliferation. *Rheumatology* 2007; 46: 1234–42.
9 Sansonno D, Tucci FA, Lauletta G *et al.* Hepatitis C virus productive infection in mononuclear cells from patients with cryoglobulinaemia. *Clin Exp Immunol* 2007; 147: 241–8.
10 Simula MP, Caggiari L, Gloghini A, De Re V. HCV-related immunocytoma and type II mixed cryoglobulinemia-associated autoantigens. *Ann N Y Acad Sci* 2007; 1110: 121–30.
11 Harati A, Brockmeyer NH, Altmeyer P, Kreuter A. Skin disorders in association with monoclonal gammopathies. *Eur J Med Res* 2005; 10: 93–104.
12 Crowson AN, Nuovo G, Ferri C, Magro CM. The dermatopathologic manifestations of hepatitis C infection: a clinical, histological, and molecular assessment of 35 cases. *Hum Pathol* 2003; 34: 573–9.
13 Kondo Y, Sung VM, Machida K, Liu M, Lai MM. Hepatitis C virus infects T cells and affects interferon-gamma signaling in T cell lines. *Virology* 2007; 361: 161–73.
14 Kondo Y, Ueno Y, Wakui Y *et al.* Rapid reduction of hepatitis C virus-Core protein in the peripheral blood improve the immunological response in chronic hepatitis C patients. *Hepatol Res* 2011; 41: 1153–68.

15 Manns MP, Rambusch EG. Autoimmunity and extrahepatic manifestations in hepatitis C virus infection. *J Hepatol* 1999; 31 (Suppl 1): 39–42.
16 Ferri C, Antonelli A, Mascia MT *et al.* HCV-related autoimmune and neoplastic disorders: the HCV syndrome. *Dig Liver Dis* 2007; 39 (Suppl 1): S13–21.
17 Laochumroonvorapong P, DiCostanzo DP, Wu H, Srinivasan K, Abusamieh M, Levy H. Disseminated histoplasmosis presenting as pyoderma gangrenosum-like lesions in a patient with acquired immunodeficiency syndrome. *Int J Dermatol* 2001; 40: 518–21.
18 Namazi MR, Kerchner KR, Pichardo RO. Essential type II mixed cryoglobulinemia causing pyoderma gangrenosum-like ulcers. *ScientificWorldJournal* 2008; 8: 228.
19 Kondo Y, Ueno Y, Machida K *et al.* Hcv-core protein could induce th17 commitment by enhancing the stat-3 signaling. *Hepatology* 2011; 54: 1332A–A.
20 Guo ZX, Chen ZP, Zheng CL *et al.* The role of Th17 cells in adult patients with chronic idiopathic thrombocytopenic purpura. *Eur J Haematol* 2009; 82: 488–9.
21 Zhao L, Tang Y, You Z *et al.* Interleukin-17 contributes to the pathogenesis of autoimmune hepatitis through inducing hepatic interleukin-6 expression. *PLoS ONE* 2011; 6: e18909.
22 Pan HF, Leng RX, Feng CC *et al.* Expression profiles of Th17 pathway related genes in human systemic lupus erythematosus. *Mol Biol Rep* 2013; 40: 391–9.

特集 災害における感染症とその予防対策

4．東日本大震災後にインフルエンザのアウトブレイクをどのように抑えたか

Post-tsunami outbreaks of influenza in evacuation centers in Miyagi prefecture, Japan

八田 益充*[1)]　賀来 満夫*[2)]

2011年の東日本大震災による大津波の被害は甚大であり，多くの人命および財産が失われ，家屋を失った数多くの被災者が避難所での生活を余儀なくされた。大規模災害が発生した後には感染症流行のリスクが高まることが知られているが，そのような状況の中で宮城県内の2つの避難所においてインフルエンザ集団発生事例が発生した。抗原検査により迅速に診断し，それに基づいて複合的な感染対策を早期に行ったことで2つの集団発生事例は無事収束した。その一方で，ボランティアを含めた施設外からの訪問者に対する健康管理の構築の必要性や，消毒薬などの衛生物品供給の偏りなど，避難所における感染対策の今後の課題も認められた。

Key Words：インフルエンザ／避難所／集団発生／迅速診断／複合的な感染対策

Ⅰ　はじめに

2011年3月11日に宮城県沖で発生した東日本大震災はマグニチュード9.0という国内観測史上最大の地震であった[1) 2)]。局地的な家屋の倒壊や火災だけでなく，地震直後に発生した広範囲の大津波による被害は甚大で，多くの人命および財産が失われ，家屋を失った数多くの被災者が避難所での生活を余儀なくされた。

一般的に，大規模災害が発生した後には感染症流行のリスクが高まることが知られており，込み合った避難所環境やトイレなどの衛生状態の悪化，インフラの途絶，食糧不足，医療システムの崩壊など，さまざまな要因から感染症の流行リスクが高まると言われている[3) 4)]。また，流行しうる感染症としては外傷に関連した感染症のほか，長期の避難生活にともない，インフルエンザや肺炎，感染性下痢症などさまざまな感染症が問題となる[5)]。今回の震災においても，家屋の倒壊・流出によって死者・行方不明者をはるかに上回る多数の避難者が避難所での長期生活を強いられ，衛生面や設備面での問題などから被災地における感染症の流行が震災直後から危惧された。

東北大学病院では発災後の被災地支援を継続的に行ってきたが，感染制御・検査診断学分野（以下，当分野と略す）においてもその一環として宮城県や地元保健所と共同で県内全域における避難所の感染対策支援を行ってきた。宮城県内の避難所を1つ1つ訪問していた中で2つのインフルエンザ集団発生事例を経験した[6)]ので，本稿ではそれらの事例の概要や実際に行われた感染対策について概説する。また，今回の対応の中で感じた災害後の感染対策上の課題についても少し触れたいと思う。

*東北大学大学院医学系研究科感染制御・検査診断学分野　[1)]助教　Masumitsu Hatta　[2)]教授　Mitsuo Kaku

Ⅱ　震災後の避難所において発生した2つのインフルエンザ集団発生事例

1．集団発生事例の概要とその対応

1例目の集団発生事例（以下，事例1と略す）は1,360名の避難者を収容していた気仙沼市内の大規模避難所において2011年3月下旬にかけて発生した。2例目の事例（以下，事例2と略す）は収容者数約200人の名取市内の中規模避難所において4月上旬に発生した（図1）。初発患者発生後，数日間の各々の施設内での患者発生分布を図2，3に示した。

インフルエンザの診断は鼻腔検体を用いたインフルエンザ迅速抗原検出キット（イムノクロマト法）を原則としたが，抗原検査が陰性または未施行でも臨床的にインフルエンザが疑わしい場合にはインフルエンザと診断した。いくつかの抗原検査陽性検体に対してreal-time PCR（ポリメラーゼ連鎖反応）法にてインフルエンザウイルスのサブタイプ同定も行った。

事例1では計25名（平均年齢50.2歳，男女比1：1.5）がインフルエンザAと診断され，感染率は1.8%であった。事例2でのインフルエンザA患者数は計20名（平均年齢47.2歳，男女比1：1.2）であり，感染率は10%であった。2つの集団発生事例の概要を表1にまとめた。また，事例2の患者検体からはreal-time PCR法にてインフルエンザAウイルス 香港型（H3N2）が検出・同定されたが，これは同時期に宮城県内で流行していたインフルエンザウイルスがH3N2であったとする報告[7)]と一致していた。インフルエンザと診断した場合，オセルタミビル75mg，1日2回内服にて治療を行った。

2．収束に向けた感染対策の取り組み

これらの集団発生に対する感染対策（表2）として，アルコール手指消毒薬を用いた手指衛生と咳エチケットの強化，マスクの配布，ポスター掲示（図4），有症者の個室収容などを行った。また，有症状者から半径2m以内に居た濃厚接触者や基礎疾患を有するハイリスク患者に対して，原則的にオセルタミビル75mg，1日1回内服にて曝露後予防投与も行った。オセルタミビルによる曝露

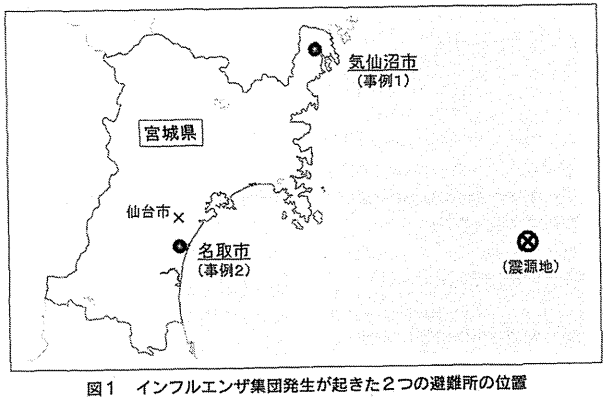

図1　インフルエンザ集団発生が起きた2つの避難所の位置
宮城県内の異なる2つの避難所においてインフルエンザ集団発生が起きた。
（筆者作成）

PCR（ポリメラーゼ連鎖反応）

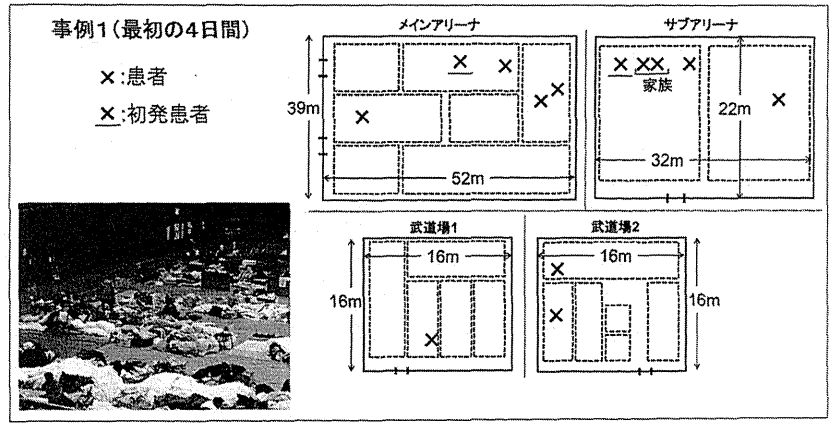

図2　事例1の患者発生分布

初発の患者が確認されてから，その周囲の人や家族に散発的に患者が発生している（写真：東北大学大学院感染制御・検査診断学提供）。

（筆者作成）

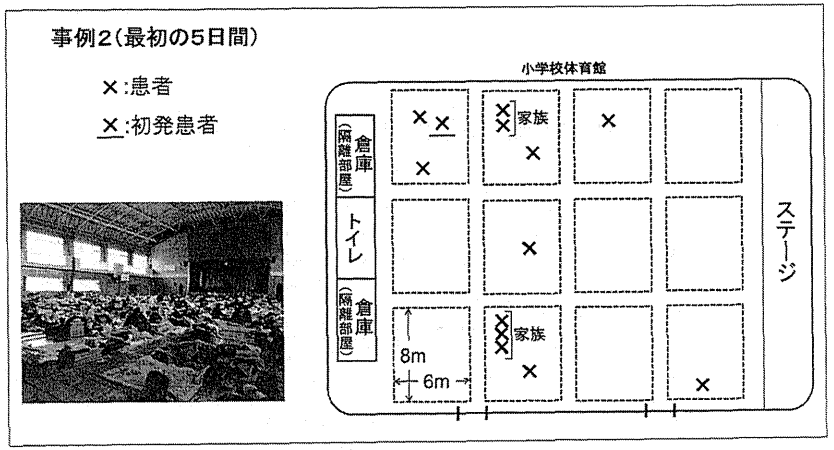

図3　事例2の患者発生分布

事例1と同様に，初発の患者の周囲の人や家族に散発的に患者が発生している（写真：東北大学大学院感染制御・検査診断学提供）。

（筆者作成）

表1　2つの集団発生事例の概要

	事例1	事例2
避難所		
場所	気仙沼市	名取市
収容人数（65歳以上の割合）	1,360名（約30%）	200名（約40%）
ライフライン	水道×，ガス×，電気○	水道×，ガス×，電気○
発症患者		
発症患者数	25名	20名
（うち抗原検査陽性者）	（15名）	（15名）
感染率	1.8%	10%
平均年齢	50.2歳（3～92歳）	47.2歳（7～80歳）
男女比	1：1.5	1：1.2

2つの事例ともに，ライフラインが障害され衛生環境がよくない状況で発生し，避難者には多数の高齢者が含まれていた。

（筆者作成）

表2　実際に行われた感染対策

- インフルエンザ患者の確実な治療と個室収容
- マスク着用，アルコール手指消毒に関する啓発の強化
- 発症者の周囲のモニタリング（新たな発症者の有無）
- 発熱外来の設置（一般診療室とは別に）
- キッズルームへの介入
- 濃厚接触者などへの抗インフルエンザ薬の予防投与

これらのうち，各避難所において実施可能なものから順次行っていった。なお，キッズルームへの介入は小児の避難者が多くキッズルームが併設されていた事例1のみに行われた。

（筆者作成）

後予防投与は，事例1では50名，事例2では34名に対して行われた。最終的に重篤な合併症や死亡者を出すことなく2事例とも収束した（図5，6）。

インフルエンザの伝播性は高く，特に閉鎖された環境では感染率が高いことが知られている。たとえば，米国海軍の船内で発生したインフルエンザ集団発生事例ではきわめて高い感染率（42%）であったことが報告されており[8]，また，2009年のパンデミックインフルエンザの際にはニューヨーク市内の学校において感染率が35%にのぼったとする報告がある[9]。今回の避難所の場合も，大勢の避難者が限られた空間の中で密集して生活せざるを得ず，インフルエンザ感染の急速な拡大が危惧された。しかし，幸いにも2つの事例ともに感染率は比較的低く，大規模な集団感染には至らずに収束した。その要因として，避難所においても有効にインフルエンザ迅速抗原検査を利用でき，かつ，複合的な感染対策を迅速に行えた点が大きかったと考えている。

インフルエンザ迅速抗原検査については，今回の2つの事例において患者の約半数以上が迅速抗原検査キットにてインフルエンザAと診断されたが，その迅速性や簡便性，高い特異性は避難所においてもすみやかな診断および対処を可能とし，

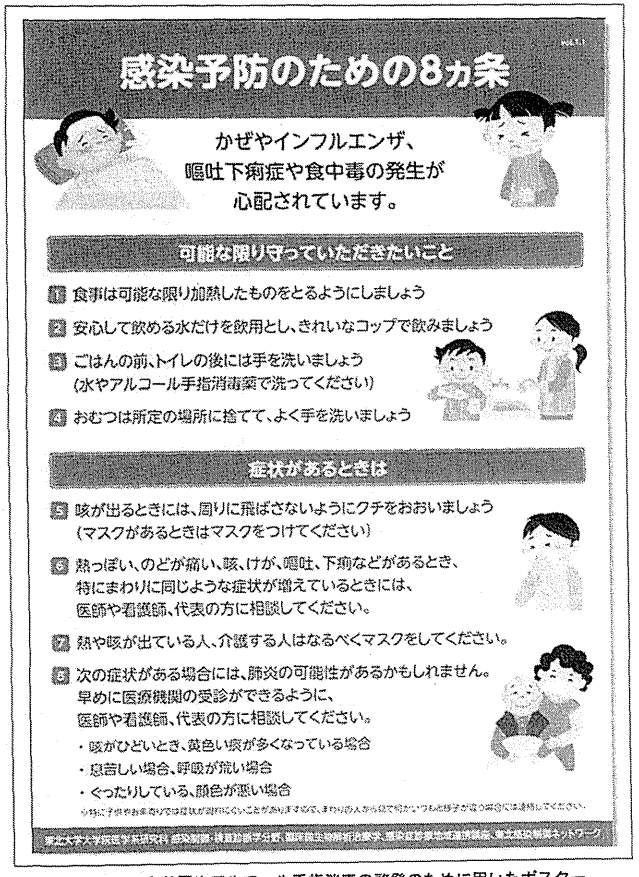

図4　マスク着用やアルコール手指消毒の啓発のために用いたポスター

なるべく目立つように，そしてひと目でわかりやすいようにイラストをつけた。ポスターは毎日，人の目に触れやすい場所に貼るように工夫し，たとえば，食事配給で並ぶ場所，トイレの扉，県や町役場などからの重要な連絡事項を貼る場所，出入り口などに掲示した。

（東北感染制御ネットワーク提供）

今回の集団発生事例においても抗原検査の結果をもとに迅速に感染対策を実施できた点できわめて有用であった。また，感染対策として抗インフルエンザ薬による曝露後予防投与と手指衛生やマスクの着用など，薬剤以外の基本的な感染対策（non-pharmaceutical interventions：NPI）を実施可能なものから漸次行っていったが，単独ではなく，これらを組み合わせて複合的に感染対策を

NPI (non-pharmaceutical interventions)

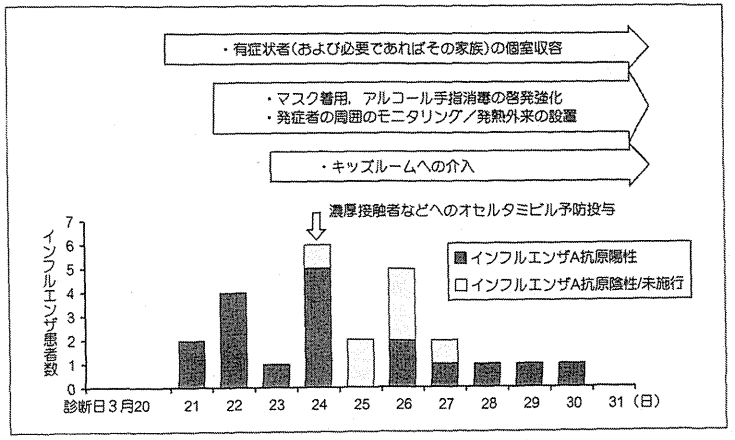

図5　事例1での流行曲線と感染対策の実施時期

事例1では，当初はマスク着用やアルコール手指消毒薬の啓発強化などを行っていたが，避難所の規模が大きく収束は困難であると判断し，濃厚接触者などへのオセルタミビル予防投与も行われた。

（筆者作成）

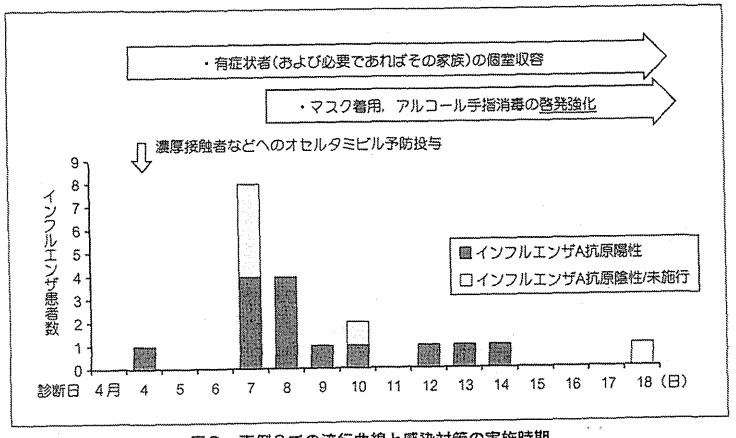

図6　事例2での流行曲線と感染対策の実施時期

事例2では，当初から濃厚接触者などへのオセルタミビル予防投与が積極的に行われたが，やはり予防投与のみでは不十分であり，その後も新規患者発生が続いたため，マスク着用・手指衛生の啓発を再度強化した。

（筆者作成）

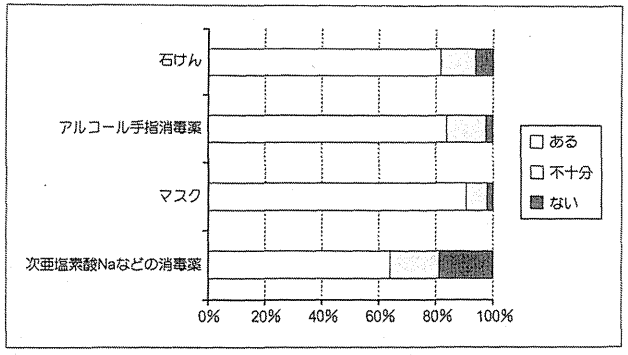

図7　宮城県内の避難所における衛生維持に必要な物品の充足度

2011年3月22日～4月1日（発災後2～4週間）の期間で宮城県内の避難所342施設に対しアンケート形式で調査を行った。アルコール手指消毒薬やマスクはおおむね充足傾向にあるのに対し，次亜塩素酸Naなどの環境消毒に必要な消毒薬が不足している避難所が多かった。

（東北大学大学院医学系研究科感染制御・検査診断学分野/感染症診療地域連携講座データより）

行っていった点も重要であったと考えている。たとえば，事例1では当初からのNPIの徹底のみでは感染拡大を抑えきれない傾向があると判断されたため，曝露後予防内服も並行して行うことで結果的に集団発生を収束することができた。逆に事例2では当初より曝露後予防投与が開始されたが，やはりそれのみでは不十分で，新たな患者発生を抑えられなかったためNPIの徹底を再度行ったことで結果的に無事収束した。

病院など医療機関での感染対策においては，有効な感染対策をいくつか組み合わせて実施する，いわゆるケアバンドルと称される複合的な感染対策の実施が近年求められている。今回の事例では，避難所で医療リソースがある程度限られるという特殊状況にありながら，迅速に複合的な感染対策を実施することで集団発生の終息につながったが，災害時の避難所においても医療機関と同様の総合的な感染対策の重要性が示唆された。

その他の無事収束した要因として，アルコール手指消毒薬による手指衛生やサージカルマスクの着用が避難所という非医療現場においてもある程度理解され順守されていた点もあげられる。この背景には一般市民のあいだで手指消毒や咳エチケットの概念が少しずつ浸透してきている印象があり，たとえば2009年のパンデミックインフルエンザのよい意味での影響であったとも考えている。

Ⅲ　避難所における感染対策の課題

この2つの避難所に共通した感染対策上の問題点として，①密集した生活環境のため個人・家族間の距離が近かったこと，②身内や知人，ボランティアなど施設外からの人の出入りが多かったこと，③手洗いなどの水道が使えず，換気が不十分であり衛生環境がよくなかったこと，④避難者には多数の高齢者が含まれていたといった点があげられた。これらは今回の2つの避難所に限らず，多くの避難所で同様であったと推測される。特に，身内や知人，ボランティアなど不特定多数が避難所に出入りする状況では，それらの訪問者の健康状態をチェックするシステムはほとんどなく，避難所に出入りする訪問者から避難所に何らかの感染症が持ち込まれる可能性がある点は重要な

問題点であると考えられた。今後の災害時の対策の課題のひとつとして避難所への訪問者などに対する何らかの健康管理体制の構築が必要である。

その他，供給物品に偏りが認められた点もひとつの大きな課題であった。当分野では避難所への感染対策支援活動に際し，避難所における衛生状態の現状を把握する目的で県内全域の避難所を対象とした避難所生活における感染管理上のリスクアセスメント調査を行った。その調査結果の一部を図7に示したが，アルコール手指消毒薬やサージカルマスクの供給状況はおおむね良好な避難所が多かった一方で，次亜塩素酸ナトリウムなど清掃や環境の消毒に必要な物品が不足している施設が多かった。今回の2つのインフルエンザ集団発生事例においては直接的な影響はなかったものの，一部の避難所ではウイルス性胃腸炎の集団発生を認めたとの報告[10]もあることから，衛生維持に必要な物品として次亜塩素酸ナトリウムなどの消毒薬についても供給の偏りが生じないよう注意して行く必要があると考えられた。

Ⅳ　おわりに

本稿を終えるに当たり，賀来 満夫教授の指揮の元でチーム全体として感染対策支援活動をともに行いました，東北大学大学院医学系研究科感染制御・検査診断学分野および感染症診療地域連携講座の先生方，避難所の医療系ボランティアや地元医療スタッフの方々，地元保健所や宮城県保健福祉部疾病・感染症対策室の方々，インフルエンザウイルスのサブタイプ同定にご協力いただいた東北大学医学部微生物学教室の方々に深く感謝申し上げます。

文　献

1) Shibahara S：The 2011 tohoku earthquake and devastating tsunami. Tohoku J Exp Med **223**：305-307, 2011.
2) Satomi S：The Great East Japan Earthquake：Tohoku University Hospital's efforts and lessons learned. Surg Today **41**：1171-1181, 2011.
3) Connolly MA, et al：Communicable diseases in complex emergencies：impact and challenges. Lancet **364**：1974-1983, 2004.
4) Waring SC, Brown BJ：The threat of communicable diseases following natural disasters：a public health response. Disaster Manag Response **3**：41-47, 2005.
5) 日本感染症学会．東日本大震災－地震・津波後に問題となる感染症－Version 2＜http://www.kansensho.or.jp/disaster/disaster_infection_v2.html＞．
6) Hatta M, et al：Post-Tsunami Outbreaks of Influenza in Evacuation Centers in Miyagi Prefecture, Japan. Clin Infect Dis **54**：e5-e7, 2012.
7) 押谷仁ほか：東日本大震災後の仙台市およびその周辺でのインフルエンザのモニタリング．病原微生物検出情報 **32**：S6, 2011.
8) Earhart KC, et al：Outbreak of influenza in highly vaccinated crew of U.S. Navy ship. Emerg Infect Dis **7**：463-465, 2001.
9) Lessler J, et al：Outbreak of 2009 pandemic influenza A (H1N1) at a New York City school. N Engl J Med **361**：2628-2636, 2009
10) 国立感染症研究所ほか：福島県郡山市の避難所における嘔吐・下痢症集団発生事例．病原微生物検出情報 **32**：S8, 2011.